ISSN 1810-2328, Journal of Engineering Thermophysics, 2024, Vol. 33, No. 2, pp. 250–268. © Pleiades Publishing, Ltd., 2024.

Heat Transfer during Boiling in Horizontal Layers of HFE-7100 on Smooth and Modified Surfaces

D. A. Shvetsov[1*], A. N. Pavlenko[1], and V. I. Zhukov[1,2]

[1] *Kutateladze Institute of Thermophysics, Siberian Branch, Russian Academy of Sciences, Novosibirsk, Russia*

[2] *Novosibirsk State Technical University, Novosibirsk, Russia*

Received December 4, 2023; in final form, April 9, 2024; accepted May 20, 2024

Abstract—Experimental data were obtained on heat transfer in horizontal layers of dielectric liquid HFE-7100 of various heights at atmospheric pressure. The heat transfer during boiling was studied on a smooth stainless steel surface and on a capillary-porous stainless steel coating manufactured by the SLM/SLS 3D printing technology. Comparison of the values of temperature pressure and critical heat flux on the smooth surface and on the capillary-porous coating has shown that in HFE-7100 layers with height below 6 mm, the heat transfer regime changes from pool boiling to boiling in thin layers of liquid. At a heat flux density of 100 kW/m^2, the temperature difference obtained on the capillary-porous coating was six times lower than that on the smooth surface.

DOI: 10.1134/S1810232824020024

1. INTRODUCTION

The boiling process is an efficient way to cool heated surfaces in a number of technical devices (thermosiphons, vapor chambers, heat pipes for various purposes, etc.). The process of boiling of dielectric liquids is now under active study as a method of cooling microelectronics and microchips, in particular in two-phase immersion cooling, due to the ability of the liquid-vapor phase transition to remove high heat fluxes at a low temperature difference between the heated surface and the liquid. Two-phase immersion cooling is a relatively inexpensive method because it does not require a complex system for coolant circulation and thus labor-intensive maintenance [1–3]. Two-phase immersion cooling is also one of the most efficient ways to reduce energy consumption during cooling [4]. The use of thin layers of liquid makes it possible to reduce coolant consumption and the weight and size characteristics of heat exchangers. To date, there are no studies aimed at analysis of heat transfer during boiling in thin horizontal layers of the commonly used dielectric liquid HFE-7100.

Using various modified heating surfaces can significantly increase the values of the heat transfer coefficient (HTC) and critical heat flux (CHF) during boiling, making this cooling method much more efficient and safe. Selection of optimal parameters of the heating surface and the properties of the working fluid should base on consideration of the physical mechanisms of heat transfer during boiling.

1.1. Influence of Liquid Layer Height on Heat Transfer during Boiling

Work [5] presents a brief review of studies and analysis of the influence of the liquid layer height on the HTC and CHF values during boiling and evaporation in thin horizontal layers of liquids.

Works with water and organic liquids [6, 7] have shown that at a certain layer height, different for each liquid, the HTC values achieved are higher than those in a large volume. In [8–10], boiling in thin films of oxygen, nitrogen, hydrogen, and helium was experimentally studied. Based on the experimental data obtained, it was established that the intensity of heat transfer during boiling in a thin film can exceed the intensity of heat transfer during pool boiling in almost the entire

*Corresponding author. E-mail: shvetsov.kh301@ya.ru

range of heat flux densities up to the onset of a boiling crisis. The authors of [8–10] refer the significant intensity of heat transfer in thin layers of liquid to the lower thermal resistance of the film as compared with the thermal resistance of the thermal boundary layer, which determines the HTC during free convection in a large volume. In experiments with distilled water, ethyl alcohol, and freon-113 at atmospheric pressure [11], it was found that increase in the liquid level above a certain value had a little effect on the HTC values, and when the level decreased, intensification of heat transfer was observed.

The works by Tolubinskii [12, 13] show the experimental dependence of the number of active nucleation sites on the thickness of the liquid film. In [14], the heat transfer and CHF were studied during evaporation of a thin layer of liquid on structures made of metal mesh, perforated screens, and copper felt (35 types of structures in total). The capillary structures under study were attached to the heat-releasing surface of 28 mm in diameter. The liquid level in the working chamber was maintained at 1–2 mm below the level of the heat-releasing surface, but the structures under study were completely covered by the liquid supplied by capillary forces. The experiments have shown that with optimal types of capillary structures, higher CHF values can be removed in thin layers of liquid as compared with pool boiling of liquid on an uncoated surface.

For water, the influence of the liquid layer height on the HTC values during boiling is shown in the works by Pioro [15, 16]. Works [17, 18] present studies in more detail on the effect of the water film thickness on the heat transfer and CHF during boiling under atmospheric pressure conditions.

In a series of works with mineral vacuum oil as a working fluid [19–23], experimental data were obtained on the HTC and CHF values, and geometric and kinematic characteristics of the structures formed in liquid layers at changes in the heat flux density and layer height.

Works [24–26] present experimental results on heat transfer in layers of n-dodecane. Data on the HTC and CHF values are presented; maps of hydrodynamic regimes were constructed; experimental data obtained in layers of liquid on a smooth surface were compared with calculated dependencies for pool boiling conditions.

1.2. Intensification of Heat Transfer during Boiling on Capillary-Porous Coatings

It is known that capillary-porous coatings intensify heat transfer during boiling, leading to low temperature differences of boiling onset and increase in the HTC and CHF values [27–29]. Work [30] shows that the presence of porous coatings leads to increment in the CHF values due to better capillary liquid replenishment. To describe, predict, and optimize the heat transfer processes during boiling on capillary-porous coatings, it is necessary to simulate the distribution of liquid-vapor flows in the heating zone. Several mechanisms established during pool boiling of liquid can be used as guidelines in choosing the geometric parameters of microstructured capillary-porous coatings.

Liter and Kaviany in [31], when designing the profile of capillary-porous coatings, suggested that thickness-modulated porous coatings can increase the HTC and CHF values due to the physical separation of ascending vapor flows and descending liquid flows. This approach is based on the idea that liquid is supplied from the volume to the tops of the thickness-modulated coating, and vapor is released from the inter-rib depressions of the coating. The liquid-vapor flows move countercurrently. The creation of separate alternating areas with low resistance to vapor escape (bubble separation) and sufficient replenishment with the liquid from the tops of the ribs of the modulated capillary-porous structures made it possible to increase the HTC values by almost two times and the CHF values by three times in comparison with a smooth surface without coatings. Min et al. in [32] studied pool boiling of n-pentane at atmospheric pressure on thickness-modulated porous coatings and found that HTC values achieved on 2D modulated porous coatings were higher than those on 3D modulated coatings. Capillary-porous 2D coatings in [33] also showed higher HTC values in comparison with microchannels with polished surface, porous coating of uniform thickness, and 3D structures.

The 3D printing technology enables production of almost any coating and formation of various structures of given porosity for study of heat transfer during boiling. In the 3D printing technology, a product is made by applying and laying down layers of powdered material, each layer being a thin cross-section of the product. Owing to precise control of the parameters of the structures in [34, 35], the influence of the parameters on the heat transfer during pool boiling of liquid was studied in detail. Data on heat transfer during boiling in thin horizontal layers of n-dodecane on a capillary-porous coating are presented in [36, 37].

1.3. Studies of Effect of Modified Surface on Heat Transfer during Pool Boiling of Dielectric Liquid HFE-7100

Fluorocarbons (FCs) and hydrofluoroethers (HFEs) are used in cooling of microelectronics. These liquids have an advantage of their saturation temperatures at atmospheric pressure (61°C) allowing maintenance of high-performance processor chips at temperatures below 85°C. These liquids do not conduct electric current, are chemically inert, and have no toxic effect on the environment [38]. In study [39], performed on a smooth copper surface, it was shown that higher values of the coefficients of surface tension and latent heat of vaporization of HFE-7100 led to HTC and CHF values higher by (50–60)% and (30–40)%, respectively, than those for FC-72. Currently, there are no studies on heat transfer enhancement during evaporation and boiling in thin horizontal layers of dielectric liquids. Analysis of literary sources shows that a large array of experimental data has been accumulated for pool boiling of liquid HFE-7100.

In [40], the effect of a stainless steel mesh coating on heat transfer was studied. The size of the heating surface was 80×15 mm^2. In [40], it was found that at low heat flux densities, a lower temperature difference was achieved on the coating as compared with an uncoated surface, but the CHF values on the coating were significantly lower than those during boiling on the uncoated surface. In [41], experiments were carried out on pool boiling of saturated and subcooled HFE-7100 on a porous graphite surface measuring (10x10) mm^2. The results of [41] were compared with data obtained on a smooth copper surface of the same dimensions. It was found that the CHF values for HFE-7100 on the porous graphite surface were 60% higher than those on the smooth copper surface. The temperature difference values at given heat flux densities on the porous graphite surface were by 25% lower than those on the smooth copper surface.

In [42], a study of heat transfer during pool boiling of HFE-7100 on sintered porous copper coatings of various thicknesses (100 μm, 360 μm, and 700 μm) was carried out. The copper particle size ranged from 5 μm to 20 μm. The size of the heating surfaces was 2×10 mm^2. The authors of [42] compared the experimental data obtained on porous coatings with data obtained on uncoated copper surfaces with the roughness $R_a = 0.78$ μm and $R_a = 0.33$ μm. It was found that the values of the boiling-onset temperature differences achieved on microporous coatings (3–11)°C were lower than those on uncoated surfaces (17–38)°C, due to the presence of a large number of cavities of (1–5) μm in size. This result is consistent with the theoretical range of active pore sizes calculated by the Hsu model [43]. In comparison with smooth surfaces, the HTC values on microporous coatings increased by (50–270)% in dependence on the coating height. The highest HTC values were achieved on a coating with height of 700 μm. The CHF values also grew by (33–60)% for microporous coatings as compared with smooth surfaces.

In [44], a study was conducted on the heat transfer during pool boiling of HFE-7100 on copper foam coatings of various thicknesses (1 mm, 2 mm, and 3 mm). The size of the heating surfaces was 16×16 mm^2. The authors of [44] compared the experimental data obtained on the copper foam with the data obtained on a copper surface with the roughness $R_a = 0.14$ μm. It was found that at heat flux densities below 200 kW/m^2, the HTC value achieved on the copper foam 2 mm thick was higher than that on the other heating surfaces studied. At heat flux densities of more than 200 kW/m^2, the highest HTC value was achieved on the copper foam 1 mm thick. The HTC values obtained on the copper foam were by 145% higher than those obtained on the smooth copper surface. The authors of [45] studied the heat transfer during pool boiling of HFE-7100 on surfaces with square copper pillars. In [45], the height and number of these pillars varied. The size of the heating surfaces was 16×16 mm^2. It was found that the highest HTC values were achieved on surfaces with the largest number of square pillars with height of 200 μm. The HTC value achieved on these surfaces was by 260% higher that the HTC value achieved on the smooth copper surface. In [46], the surfaces with square pillars from [45] were covered by Al_2O_3 particles. The hierarchically structured surfaces obtained in this way made it possible to increase the HTC values by another 65%.

In [47], the heat transfer during pool boiling of HFE-7100 on porous Al_2O_3 films on aluminum substrates was studied. The size of the heating surfaces was 25×25 mm^2. The authors of [47] failed to obtain HTC or CHF values higher than those on smooth aluminum surfaces for both horizontal and vertical orientations of the heater. The analysis of experimental results carried out by the

authors of [47] revealed that the pore size of the Al_2O_3 films was (0.02–0.07) μm and was too small for these pores to be activated. As was shown in [42], according to the Hsu model [43], the optimal size of active pores for boiling of HFE-7100 must be about (1–5) μm.

In [48], a study of the heat transfer during pool boiling of HFE-7100 on copper and titanium surfaces covered by TiO_2 nanotubes was carried out. The size of the heating surfaces was 2×10 mm^2. The authors of [48] compared the experimental data obtained on the copper and titanium surfaces covered by nanotubes with the data obtained on the smooth copper and titanium surfaces. The temperature difference values obtained on the smooth copper and titanium surfaces were slightly different, but the highest CHF was obtained on the smooth copper surface. It was found that the CHF values obtained on the copper surface covered by nanotubes and the titanium surface covered by nanotubes could be as high as 52.2 W/cm^2 and 48.9 W/cm^2, respectively, which is approximately by 40% higher than that on the corresponding smooth surfaces. The effect of the nanotube coating on the HTC value was completely different for the copper and titanium surfaces. The titanium surface covered by nanotubes had HTC values higher by 65% than those of the smooth titanium surface. A copper surface covered by nanotubes showed the opposite effect, i.e., HTC values by 20% lower than those for the smooth copper surface. The authors of [48] refer this effect to the higher thermal resistance between the copper surface and TiO_2 nanotubes.

The influence of the roughness of a copper heating surface and operating pressure on the heat transfer during pool boiling of HFE-7100 was studied in detail in [49, 50]. The diameter of the heating surface was 30 mm and 40 mm in [49] and [50], respectively. In [49, 50], close HTC and CHF values were obtained for different pressures. It was established that increase in the roughness Ra from 0.023 μm to 1.878 μm [49] and from 0.019 μm to 0.587 μm [50] led to higher HTC and CHF values. Rise of pressure on all copper surfaces considered in [49, 50] also led to growth of the HTC and CHF values. In [51], copper plates with different roughness were drilled through for creation of artificial nucleation sites and attached to the top of the heater. The size of the copper surfaces was 30×30 mm^2. The diameter of the holes and the distance between them varied for each plate. It was established that on the copper plate without holes with the greatest roughness$R_a = 7.564$ μm, the HTC values achieved were by 150% higher than those on the smooth surface with the lowest roughness $R_a = 0.48$ μm. On the plate with the roughness $R_a = 7.564$ μm with a row of holes with diameter of 1 mm and spacing of 3.5 mm between them, the HTC values achieved were by 124% higher than those on the plate without holes.

In [52], a study of the heat transfer during pool boiling of HFE-7100 on porous coatings in the form of sintered copper particles and copper wire meshes was carried out. The diameter of the heating surfaces was 15 mm. It was found that on the sintered porous coatings, the HTC and CHF values increased by 85% and 66%, respectively, as compared with the data obtained on the smooth copper surface. On a surface with mesh, the HTC and CHF values grew by 144% and 81%, respectively. At low heat flux densities, the smallest values of temperature difference were achieved on the sintered porous coatings, whereas at high heat flux densities, the lowest values of temperature difference were observed on the surfaces with meshes. In [53], the heat transfer during pool boiling of HFE-7100 on a porous heater with diameter of 20 mm was studied. The purpose of the experiments in [53] was to obtain a low temperature difference of boiling onset. The authors of [53] prepared a porous coating with average pore size of ~ 0.33 μm, basing on the range of active pore sizes calculated by the Hsu model [43]. As a result, the temperature difference of boiling onset on the porous coating was almost by half lower than that on a smooth surface made of indium and tin oxide.

Work [54] presents the results of a study of the heat transfer during pool boiling of HFE-7100 on structured fins created by additive SLM manufacturing. The size of the heating surfaces was 10×10 mm^2. The finless surface, 2D triangular and rectangular fins, and 3D structures were fabricated with the use of AlSi10Mg powder. The maximum values of the CHF (64.19 W/cm^2) and HTC (2.22 W/cm^2) were achieved. It is worth noting that due to the high roughness of the surfaces produced by the SLM manufacturing, nucleation sites were activated over their entire area. Due to the random formation of bubbles on the surfaces, some bubbles could merge with each other and prevent liquid replenishment to the coating. Thus, when designing a coating structure using additive manufacturing, it is especially important to ensure free and organized removal of the vapor phase from the heating surface for better liquid replenishment.

The literature review performed shows that the influence of the HFE-7100 layer height on the heat transfer during boiling was not studied. Research on the characteristic transitions from heat transfer during pool boiling of liquid to heat transfer during boiling in thin horizontal layers of liquid is necessary for designing highly efficient cooling systems for future generations of central processors. This could be a promising technology for significant reduction of the consumption of expensive HFE7100.

The vast majority of studies of boiling processes with HFE-7100 on modified surfaces use results obtained on smooth copper surfaces as a comparative basis. Conducting experiments on a stainless steel surface will give better understanding of the influence of the physical properties of the heating surface on the heat transfer during boiling of HFE7100 and will help to design new highly efficient methods for intensifying the heat transfer.

This work examines the influence of the height of a horizontal layer of HFE-7100 on the heat transfer during boiling on a microstructured 2D modulated capillary porous coating. The coating was produced by the additive 3D printing manufacturing using the SLM/SLS (selective laser melting/sintering) method. The experimental results obtained are compared with data obtained on a smooth stainless steel surface. In contrast to the studies discussed above, in this work, the heat transfer during boiling in horizontal layers of HFE-7100 is studied on lengthy heating surfaces of 120 mm in diameter.

2. EXPERIMENTAL

2.1. Experimental Setup

The studies were carried out on the experimental setup shown in Fig. 1. A detailed description of the installation is given in [36]. The working chamber is made in the form of a cylindrical vessel

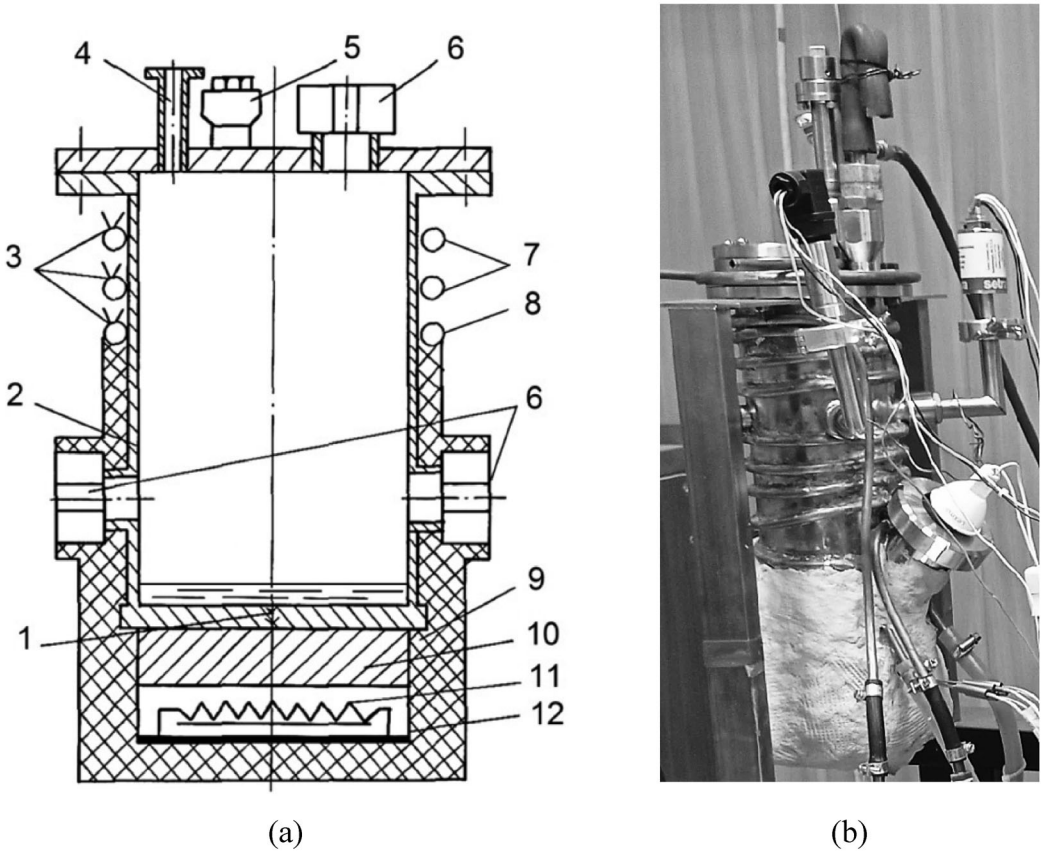

Fig. 1. (a)—Scheme of experimental setup: 1—thermocouples for measuring temperature of chamber bottom, 2—housing, 3—thermocouples for measuring temperature of cooling water, 4—pipe for attaching system for pumping and pressure measurement, 5—vacuum inlet, 6—inspection windows, 7—cooling coil, 8—heating coil, 9—thermal insulation layer, 10—copper plate, 11—electric heater, 12—electric heater casing; (b)—photograph of experimental setup.

Table 1. Thermophysical properties of HFE-7100 at pressure of 100 kPa

T_s, °C	61
ρ_l, kg/m^3	1419
ρ_v, kg/m^3	9.027
h_{lg}, J/kg	$1.117 \cdot 10^5$
ν, m^2/s	$3.008 \cdot 10^{-7}$
σ, N/m	$9.936 \cdot 10^{-3}$
λ, W/(m·K)	0.062
c_p, J/(kg·K)	1255

of steel 12X18H10T with wall thickness of 1 mm. The internal diameter of the working chamber is 120 mm and the height is 300 mm. The bottom is heated by tubular electric heater 11 with power of 3 kW. Copper plate 30 mm thick 10 located between electric heater 11 and the bottom of the working chamber, serves for uniform distribution of the heat flux directed to the heating surface. For measurement of the heat fluxes, five holes with diameter of 1.5 mm were drilled in the bottom of the working chamber in parallel to the heating surface at different heights. Copper-constantan thermocouples in stainless capillaries were inserted into these holes. The gap between the bottom and the copper plate was filled with a special paste with high thermal conductivity. The chamber was cooled by water flowing in coil 7 on the outer surface of the upper part of the working chamber. Below the cooling coil, there was additional coil 8 for heating the lower part of the working chamber to the saturation temperature of the working liquid in order to reduce the heat losses of the heater because of flows along the walls of the working chamber from the heater to the cooling coil [55]. The working chamber was equipped with six windows for visual observation of processes. The heater and the working chamber in their lower parts were thermally insulated with kaolin wool 9.

HFE-7100 was used as the working liquid. The HFE-7100 thermophysical properties presented in Table 1 were calculated according to data from [56–58]. Before the start of the experiments, a certain amount of the working liquid was poured onto the bottom of the working chamber for creation of a layer of the required height. The liquid was thoroughly degassed by boiling under reduced pressure for several hours. During the experiments, steady-state heat transfer regimes were obtained, in which temperatures along the thickness of the heated wall and the pressure above the liquid layer in the working chamber were recorded, and video recording of the process was carried out with a high-speed video camera. In the experiments, boiling curves were got at a constant pressure of 100 kPa above the liquid layer.

The smooth stainless steel surface had the roughness $R_a = 0.62$ μm ($R_z = 3.2$ μm).

2.2. Capillary-Porous Coating

The capillary-porous coating made of stainless steel LPW 155 (15-5PH) was applied to the bottom of the specially manufactured chamber by the 3D laser printing technology using the SLM/SLS (selective laser melting/sintering) method. The technology of coating application is described in detail in [36, 59]. 2D modulated structures with a sinusoidal dependence of the local coating thickness on the transverse coordinate were under consideration. The thermal conductivity of the coating material is $\lambda \approx 20$ W/(m·K) [60]. The porosity $\varepsilon = 44\%$. The maximum ridge height $\delta = 550$ μm, and the minimum height (residual layer) $\delta_0 = 50$ μm. The amplitude $A = \delta - \delta_0 = 500$ μm. The coating profile equation is $z = (A/2) \cdot \sin(2\pi x/\lambda_m) + A/2 + \delta_0$, where z is the vertical coordinate and x is the horizontal coordinate. The modulation wavelength $\lambda_m = 3.5$ mm. The morphology of the stainless steel sample was analyzed with a Hitachi S-3400N scanning electron microscope. A photograph of the coating and its SEM image are shown in Fig. 2.

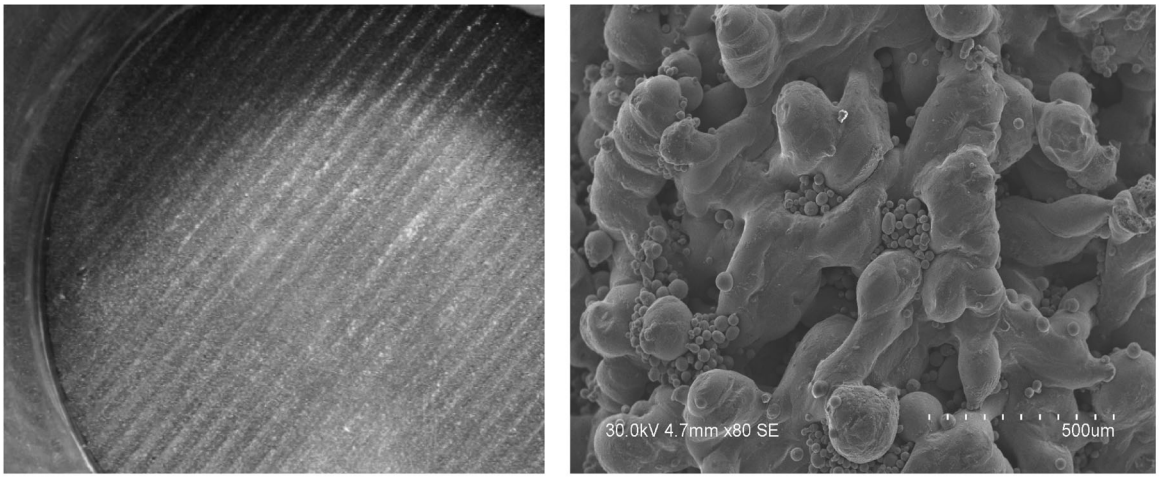

Fig. 2. Capillary-porous coating made of stainless steel: (a) photograph of top view of coating; (b) SEM image of coating.

2.3. Estimation of Measurement Uncertainty

The heat flux was calculated with application of the Fourier equation from the temperature gradient measured along the center line across the thickness of the working chamber bottom with a linear approximation of the output signal of five thermocouples:

$$q = -\lambda \left(\frac{\partial T}{\partial x} \right), \tag{1}$$

where x is the distance at which thermocouples are located along the thickness of the bottom of the working chamber, m.

The temperature of the heating surface was determined via straight-line interpolation of thermocouple readings by the least squares method with a linear regression model:

$$T = \left(\frac{\partial T}{\partial x} \right) x + T_w. \tag{2}$$

The temperature difference ΔT was determined as the difference between the temperature of the heating surface T_w and the temperature of the saturated vapor T_s. The instrument uncertainty of the pressure measurement was $\pm 0.2\%$ of the total scale.

The uncertainty ΔT_w in measuring the wall surface temperature consisted of an instrumental uncertainty of ± 0.3°C in measuring the temperature with a thermocouple and the uncertainty in measuring the value of the temperature gradient, expressed by the residual variance for determination of the parameter T_w from formula (2). The uncertainty in measuring the temperature of the heating surface was calculated according to the formula $\Delta T_w = \sqrt{(\theta_{pr})^2 + (\sigma_{T_W})^2}$, where θ_{pr} is the instrumental uncertainty of measuring the temperature with a thermocouple, °C; σ_{T_W} is the residual variance for determination of the parameter T_w from temperature gradient (1). The total uncertainty in measuring the heating surface temperature did not exceed ± 0.6°C.

The uncertainty of measuring the temperature difference between the heating surface and the saturation temperature was calculated by the formula

$$\delta(\Delta T) = \sqrt{(\Delta T_w)^2 + (\Delta T_s)^2}. \tag{3}$$

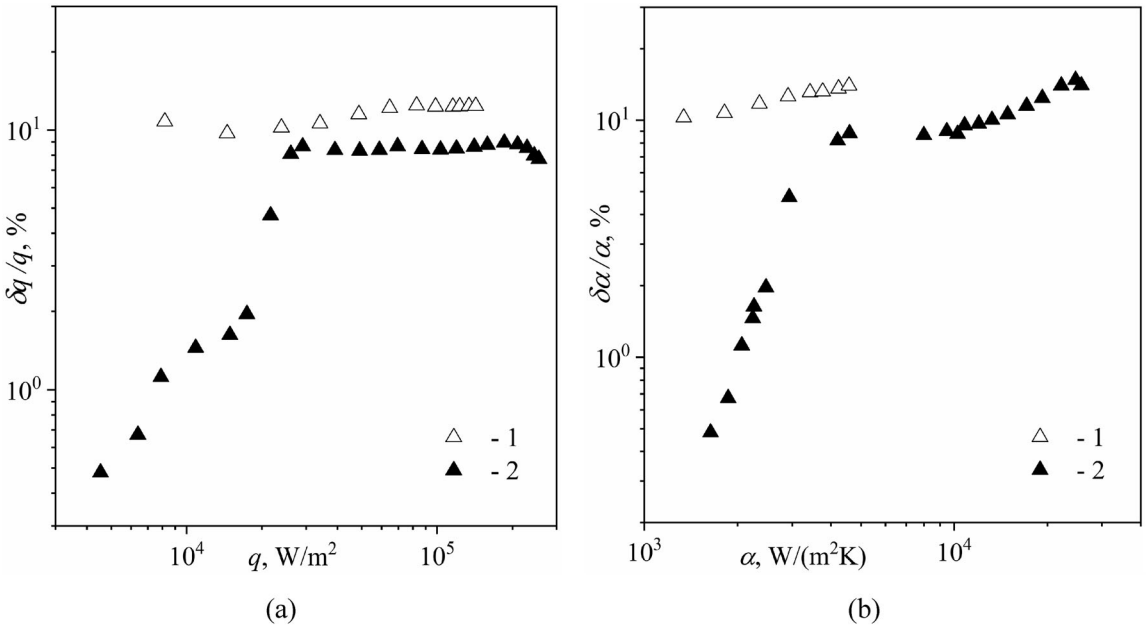

Fig. 3. Relative measurement error: (a) heat flux density; (b) heat transfer coefficient. 1—smooth surface; 2—capillary-porous coating.

The relative uncertainty in measuring this temperature difference $\delta(\Delta T)/\Delta T$ did not exceed ±7%. The thermal conductivity coefficient of steel 12X18H10T and its absolute error were calculated by the formula in [61]

$$\lambda = 10 \pm 0.47 + \left(0.164 \pm 0.2 \cdot 10^{-3}\right) \cdot (T_W + 273)\,. \tag{4}$$

For calculation of the uncertainty of heat flux measurement, the following formula was used:

$$\Delta q = \sqrt{\left(\frac{\partial q}{\partial \lambda} \cdot \Delta\lambda\right)^2 + \left(\frac{\partial q}{\partial \frac{\partial T}{\partial x}} \cdot \Delta \frac{\partial T}{\partial x}\right)^2}\,, \tag{5}$$

where $\Delta\lambda$ is the uncertainty of measuring the thermal conductivity coefficient, which was found from formula (4); $\Delta(\partial T/\partial x)$ is the residual variance for determining the temperature gradient $\partial T/\partial x$. The relative uncertainty of heat flux measurement $\Delta q/q$ did not exceed ±14% (Fig. 3a).

For calculation of the heat transfer coefficient, the following formula was used:

$$\alpha = \frac{q}{\Delta T}. \tag{6}$$

The uncertainty of HTC measurement was calculated by the formula

$$\Delta\alpha = \sqrt{\left(\frac{\partial \alpha}{\partial q} \cdot \Delta q\right)^2 + \left(\frac{\partial \alpha}{\partial \Delta T} \cdot \delta\left(\Delta T\right)\right)^2}\,. \tag{7}$$

The calculated relative uncertainty of HTC measurement $\Delta\alpha/\alpha$ at heat flux densities greater than 100 kW/m^2 did not exceed 15% (Fig. 3b).

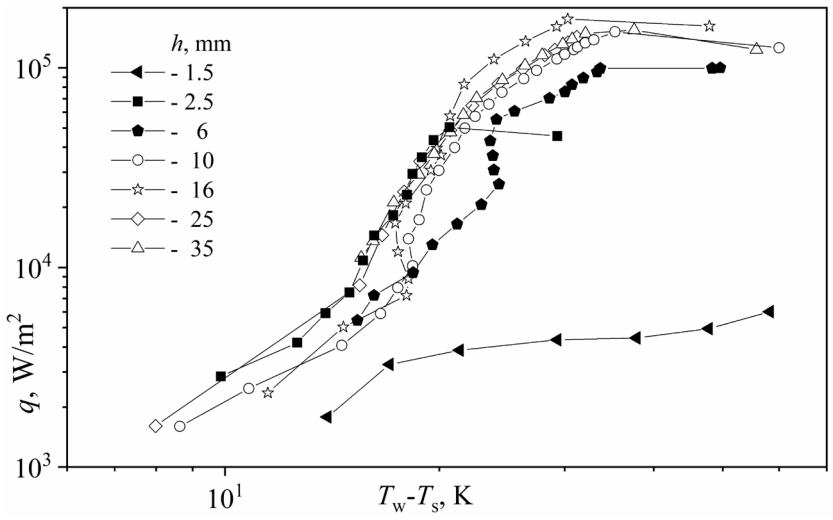

Fig. 4. Boiling curves obtained in layers of HFE-7100 of various heights at pressure of 100 kPa on smooth stainless steel surface.

3. RESULTS AND DISCUSSION

3.1. Influence of Liquid Layer Height on Heat Transfer during Boiling on Smooth Surface

Figure 4 shows the dependences of the heat flux density on the temperature difference in HFE-7100 layers with height of 1.5 mm, 2.5 mm, 6.0 mm, 10.0 mm, 16 mm, 25 mm, and 35 mm at a pressure of 100 kPa. It was found that in a layer 1.5 mm high at low heat flux densities ($q \sim 3$ kW/m^2), a dry spot appeared in the center of the surface. This led to a surge in the temperature difference with a slight growth of the thermal load. In a layer 2.5 mm high, the dry spot also appeared, but at much higher heat flux densities ($q \sim 50$ kW/m^2). The CHF values obtained in a 6 mm layer were higher than those in layers of lower height. Thus, comparison of the values of the temperature pressure and CHF shows that in HFE-7100 layers higher than 6 mm, the heat transfer regimes changed from boiling in thin layers of liquid to pool boiling. At atmospheric pressure, the capillary constant value for HFE-7100 was 0.8 mm. Accordingly, the change in the regime from boiling in thin layers of liquid to pool boiling for HFE-7100 occurred at a layer height of about seven capillary constants.

In HFE-7100 layers with heights of 10.0 mm, 25 mm, and 35 mm, the HTC and CHS values were practically the same at a pressure of 100 kPa, as can be seen from the curves in Fig. 4. The HTC and CHS values in a layer 16 mm high were higher than those in liquid layers of other thicknesses.

3.2. Comparison of Experimental Data Obtained in Liquid Layers on Smooth Surface with Dependencies Calculated for Pool Boiling Conditions

In this work, the HTC values obtained during boiling in layers of HFE-7100 of various heights on a smooth stainless steel surface were compared with the known calculated dependencies for pool boiling.

The Gogonin formula [62] takes into account the roughness and thermophysical properties of the heating surface and liquid:

$$Nu = 0.01\mathrm{Re}_*^{0.8}\mathrm{Pr}^{1/3}bK_t^{0.4}\overline{R}_z^{0.2}X^{-0.2}, \tag{8}$$

where $Nu = \frac{\alpha l_\sigma}{\lambda_l}$ is the Nusselt criterion; $l_\sigma = \sqrt{\frac{\sigma}{g(\rho_l - \rho_v)}}$ is the capillary constant, m; σ is the liquid surface tension coefficient, N/m ; g is the free fall acceleration, m/s^2; ρ_l and ρ_v is the density of liquid and vapor, respectively, kg/m^3; λ_l is the coefficient of thermal conductivity of the liquid, W/(m·K); $Re_* = \frac{ql_\sigma}{h_{lg}\rho_v\nu_l}$ is the Reynolds number; $Pr = \frac{\nu_l}{a_l}$ is the Prandtl number; $a = \frac{\lambda}{\rho_l c_p}$ is the

thermal diffusivity of the liquid, m^2/s; $K_t = \frac{(h_{lg}\rho_v)^2 l_\sigma}{c_p T_s \rho_l \sigma}$ is the Peclet criterion; $b = 1 + 10\left(\frac{\rho_v}{\rho_l - \rho_v}\right)^{2/3}$ is a dimensionless complex; $\overline{R_z} = \frac{R_z}{l_\nu}$ is the dimensionless roughness; $l_\nu = \left(\frac{\nu^2}{g(1-\rho_v/\rho_l)}\right)^{1/3}$ is the viscosity-gravitational constant of the liquid, m; $X = \frac{\lambda_l c_{pl} \rho_l}{\lambda_w c_{pw} \rho_w}$ is a dimensionless complex.

Li presents in [63] a modification of the Rohsenow formula [64], which takes into account the roughness and thermophysical properties of the heating surface and liquid:

$$\frac{c_p \Delta T}{h_{lg}} = 0.013 C_s^{-0.33} \left(\frac{q l_\sigma}{\mu h_{lg}}\right)^{0.33} \mathrm{Pr}, \tag{9}$$

$$C_s = (1 - \cos\theta)^{0.5} \left[1 + \frac{5.45}{(R_a - 3.5)^2 + 2.61}\right] \gamma^{-0.04}, \tag{10}$$

$$\theta = \mathrm{MAX}(\theta,\ 15^\circ), \tag{11}$$

where θ is the contact angle of wetting, °; $\gamma = \sqrt{\frac{\lambda_w c_{pw} \rho_w}{\lambda_l c_{pl} \rho_l}}$ is a complex; R_a is the surface roughness, μm. The contact angle of wetting of HFE-7100 is (5–10)° and thus according to formula (11), for calculation using formula (10), it is necessary to take the contact angle of wetting $\theta = 15^\circ$.

Stephan and Abdelsalam in [65] obtained the following calculated dependence for hydrocarbons:

$$Nu = 0.0546 \left[\left(\frac{\rho_v}{\rho_l}\right)^{0.5} \frac{q d_0}{\lambda_l T_s}\right]^{0.67} \left(\frac{\rho_l - \rho_v}{\rho_l}\right)^{-4.33} \left(\frac{h_{\mathrm{lg}} d_0^2}{a_l^2}\right)^{0.248}, \tag{12}$$

$$d_0 = 0.0146\theta \sqrt{\frac{2\sigma}{g\,(\rho_l - \rho_g)}}, \tag{13}$$

where d_0 is the bubble separation diameter, m. For calculation by formula (12), obtained for hydrocarbons, it is necessary to take the contact angle of wetting $\theta = 35^\circ$.

Figure 5 shows a comparison of experimental data obtained in layers of different heights at a pressure of 100 kPa on a stainless steel surface with calculated dependencies (8), (9), and (12) and experimental data from [42, 45, 49–51], obtained for pool boiling on a copper surface. Table 2 presents the roughness of the heating surfaces without coatings with which the comparison in Fig. 5 is given. The calculations using formulas (8) and (9) were performed for surfaces made of copper and stainless steel with the roughness $R_a = 0.62$ μm (this work).

Table 2. Parameters of smooth heating surfaces from various researchers

Author	Heating surface size, mm	Heating surface material	X	γ	Roughness R_a, μm
[42]	2×10	copper	$8 \cdot 10^{-5}$	111	0.33
[45]	16×16	- // -	- // -	- // -	0.14
[51]	30×30	- // -	- // -	- // -	0.48
[49]	$d = 30$	- // -	- // -	- // -	0.023
[50]	$d = 40$	- // -	- // -	- // -	0.019
This work	$d = 120$	Stainless steel	$1.5 \cdot 10^{-3}$	25	0.62

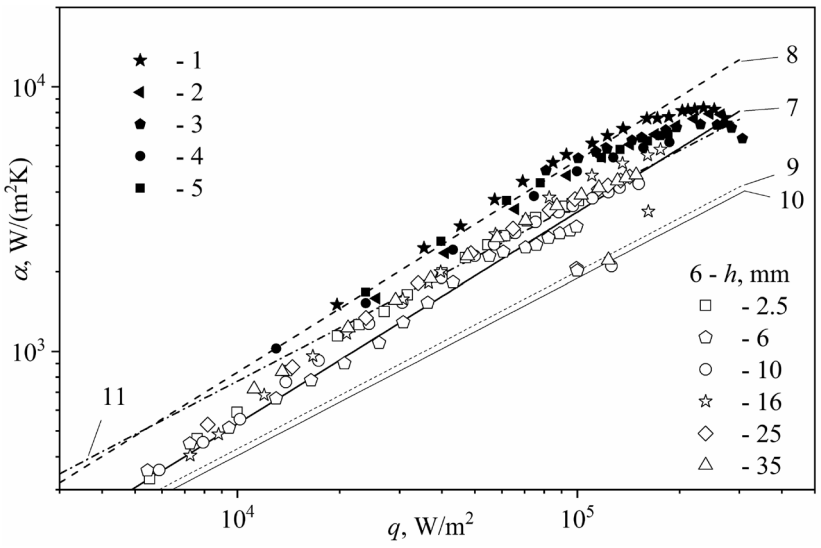

Fig. 5. Comparison of experimental data with calculated dependences at pressure of 100 kPa: 1—[42], 2—[45], 3—[51]; 4—[49]; 5—[50]; 6—data obtained in HFE-7100 layers of different heights; calculation by formula (8): 7—stainless steel, 8—copper; calculation by (9): 9—stainless steel, 10—copper; 11—calculation according to (12).

It can be seen from Fig. 5 that the experimental HTC and CHF values from works [42, 45, 49–51] for pool boiling on copper surfaces with different roughnesses in the studied range differ slightly from each other. The HTC and CHF values obtained on copper surfaces in [42, 45, 49–51] were higher than the experimental data obtained in this work on the stainless steel surface during boiling in liquid layers of different heights. In Table 2, the dimensionless complexes X and γ for copper are $8{\cdot}10^{-5}$ and 111, respectively, and those for stainless steel are $X = 1.5 \cdot 10^{-3}$ and $\gamma = 25$. Comparison of the experimental data with formula (8) shows that during boiling of HFE-7100, the increase in the dimensionless complex X when the heating surface made of stainless steel is chosen significantly reduces the HTC values. Since $\gamma = \frac{1}{\sqrt{X}}$, it follows from formula (9) that the HTC values on the stainless steel surface must be higher than those on the copper surface, that is, the opposite trend is observed. However, in the same work by Li [63] it is shown that at $\gamma > 5$, the influence of the thermophysical properties of the heating surface can be neglected, and, therefore, variation of the γ value has little effect on the HTC values.

From Fig. 5 it follows that dependence (8) correlates well with the experimental data for both stainless steel and copper surfaces. As proposed in [62] (formula (8)), an exponent of 0.8 at the heat flux density describes well the experimental data of various researchers in the range from low heat flux densities up to $q \sim 200$ kW/m^2.

Dependence (9) lies below all experimental data and is in weak correlation with them. Dependence (11) correlates well with the experimental data obtained on the smooth stainless steel surface at $q > 50$ kW/m^2.

The analysis done shows that the thermophysical properties of the heating surface material have a significant influence on the heat transfer during boiling of HFE-7100. It was established that the HTC and CHF values on the smooth surface made of stainless steel were lower than those on the smooth surface made of copper.

3.3. Influence of Liquid Layer Height on Heat Transfer during Boiling on Microstructured Capillary-Porous Coating

Figure 6 shows dependences of the heat flux density on the temperature difference, obtained in layers with height of 1.5 mm, 2.5 mm, 6.0 mm, 10.0 mm, and 25 mm at a pressure of 100 kPa. It was found that at low heat flux densities ($q \sim 2$ kW/m^2), a dry spot appeared in a layer 1.5 mm high, with the formation of a ring of very small bubbles around it. With the formation of a large number of small bubbles, there was a sharp fall in the temperature pressure at increase in the heat

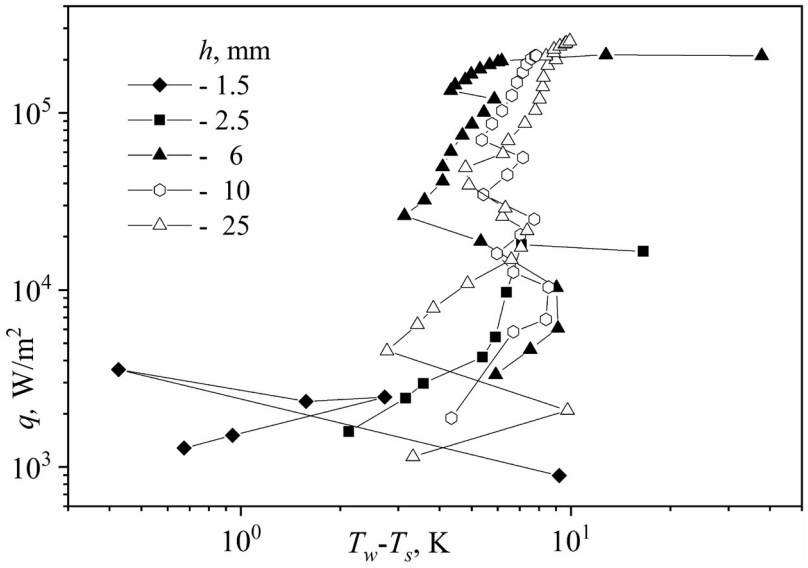

Fig. 6. Boiling curves obtained in layers of HFE-7100 of various heights at pressure of 100 kPa on 2D modulated capillary-porous stainless steel coating.

flux density [36, 59], and the boiling curve had a loop-like shape (Fig. 6). With further increase in the thermal load, the liquid layer completely evaporated from the heating surface. In a layer 2.5 mm high, the dry spot appeared at higher heat flux densities ($q \sim 15$ kW/m^2). On the smooth surface, the dry spot in the layer 2.5 mm high appeared at $q \sim 40$ kW/m^2 (Fig. 4).

From Fig. 6 it is clear that at $q > 20$ kW/m^2, the temperature pressure values achieved in a layer of liquid 6 mm high were lower than those in thicker layers. Apparently, with increase in the liquid layer height, the fraction of the heat flux removed due to evaporation decreases, and the fraction of the heat flux removed due to natural convection grows [26], and this leads to higher values of temperature difference in thicker layers of liquid.

In liquid layers 10 mm and 25 mm high, the CHF values obtained were higher, whereas the temperature pressure values in these layers were exceeded those in a layer 6 mm high. At $q \sim 200$ kW/m^2, a dry spot appeared in a layer 6 mm high, and the temperature pressure values surged. So, comparison of the values of temperature pressure and heat transfer coefficient on the capillary-porous coatings and the smooth surface has shown that in HFE-7100 layers with height below 6 mm, the heat transfer regime changes from pool boiling to boiling in thin layers of liquid.

Figure 7 presents photographs of boiling in a layer 6 mm high at $q \sim 100$ kW/m^2 on the smooth and modified surfaces. At the heat flux density $q \sim 100$ kW/m^2, the temperature difference values obtained on the capillary-porous coating were six times lower than those on the smooth surface. The space between the ridges of the coating provided free organized removal of vapor during boiling, and the liquid was replenished through the tops of the ridges. When nucleation sites were activated on the stainless steel coating at a large temperature gradient from the base to the top of the ridge, intensification of the heat transfer was observed. On the smooth surface at $q \sim 100$ kW/m^2 in a layer 6 mm high, large bubbles formed in the center. As the heat flux density grew, the dry spot formed in the place of the large bubbles. The two-dimensional instability of a finite-height horizontal layer of boiling liquid on various heating surfaces is discussed in detail in [67].

It is worth noting that the results were obtained on a "run-in" capillary-porous coating. The features of heat transfer on a "run-in" and "unrun" coatings can be explained as follows: before the experiments, some pores of the coating might contain no vapor-gas phase. Instead, they were filled with liquid and were activated only at high heat flux densities. When pre-crisis heat flux values were reached, all pores were apparently activated. The boiling curves on a "run-in" coating shift to the left, towards smaller temperature differences, but the CHF value remains practically unchanged [37, 66].

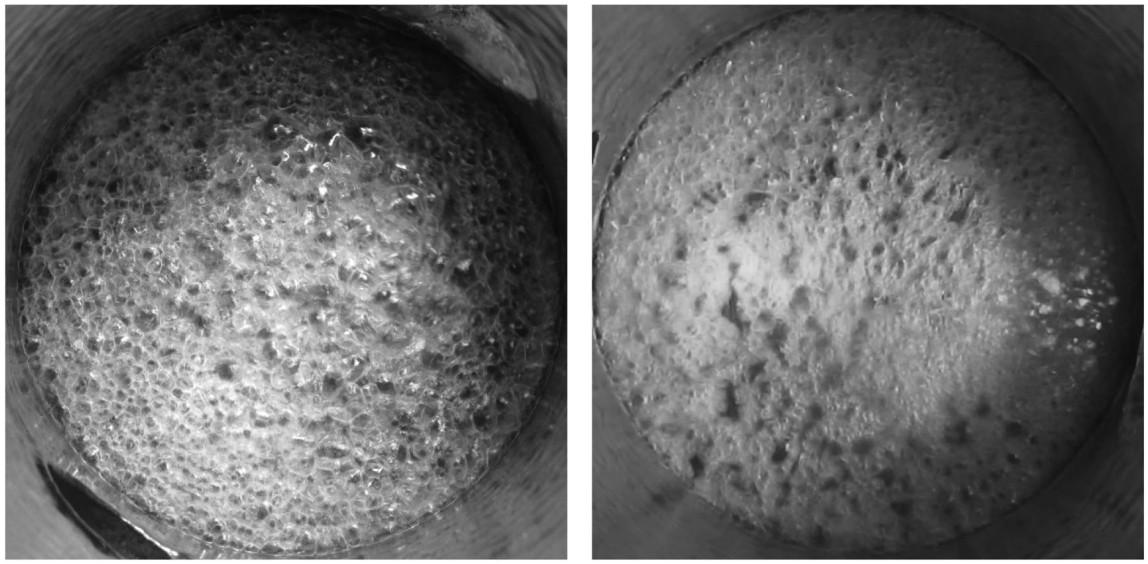

Fig. 7. Photographs of heat transfer process in HFE-7100 layer 6 mm high: (a) boiling on modified surface, $q = 100.9$ kW/m^2, $T_w - T_s = 5.4$ K; (b) boiling on surface without coating, $q = 99.4$ kW/m^2, $T_w - T_s = 33.6$ K.

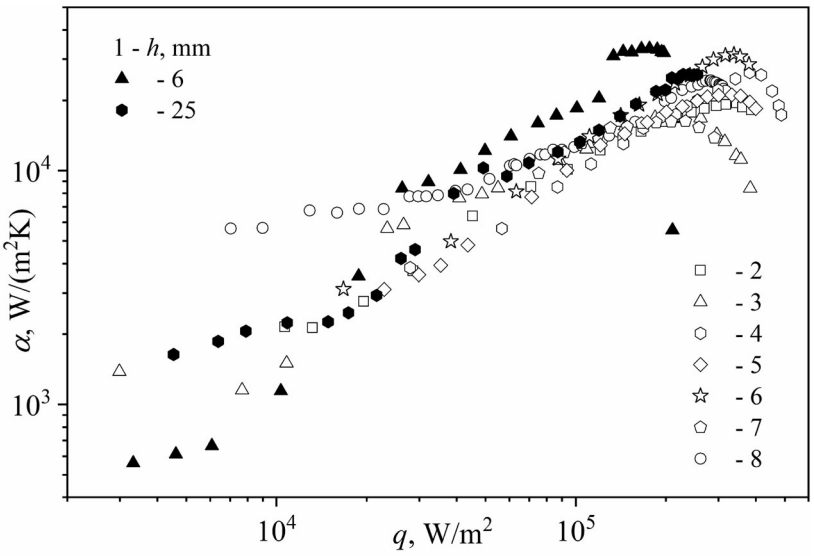

Fig. 8. Comparison of experimental data: 1—data obtained in layers 6 mm and 25 mm high on capillary-porous stainless steel coating; data from 2—[44]; 3—[42]; 4—[48]; 5—[45]; 6—[46]; 7—[51], 8—[41].

3.4. Comparison of Experimental Data Obtained in Layer of Liquid on Capillary-Porous Coating with Experimental Data for Pool Boiling Conditions

Figure 8 presents a comparison of the experimental data obtained in layers 6.0 mm and 25 mm high on the capillary-porous stainless steel coating with the experimental data for pool boiling conditions from works [41, 42, 44–46, 48, 51]. Table 3 provides a comparison of the experimental maximum HTC values obtained on various modified surfaces. It is shown that in this work, the HTC values obtained during boiling in an HFE-7100 layer 6 mm high on the 2D modulated capillary-porous stainless steel coating ($\alpha \sim 33$ kW/(m^2·K)) were higher than those in works [41, 42, 44–46, 48, 51] in pool boiling of liquid.

Table 3. Comparison of experimental data obtained on various modified surfaces

Author	Brief description of surface	Size, mm	Material of modified surface	Maximum HTC at respective heat flux	
				$\alpha_{\max}$, kW/(m^2·K)	q,kW/ m^2
[44]	Metal foam	16×16	Copper	19.5	345
[42]	Sintered coating of uniform thickness	2×10	Copper	16.9	184.3
[48]	Nanotubes	2×10	TiO_2 on titanium substrate	26.3	381.6
[45]	Square pillars	16×16	Copper	21.1	332.3
[46]	Square pillars covered by porous structures	16×16	Copper coated with Al_2O_3	31.4	338
[51]	Rough plate with holes	30×30	Copper	16.3	232.6
[41]	Coating of uniform thickness	10×10	Graphite	24.3	283.6
This work, layer 6 mm	2D coating of modulated thickness	$d = 120$	Stainless steel	**33.3**	**176.6**

The growth of the fraction of the heat flux removed by evaporation in a thin layer of liquid also led to higher HTC values as compared with those obtained in a large volume. However, Fig. 8 shows that in an HFE-7100 layer 6 mm high, the CHF value is on average two times lower than that in a layer 25 mm high and in a large volume of liquid.

Thus, in this work, acceptable geometric parameters and material of a capillary-porous coating were selected for enhancing the heat transfer during boiling of HFE-7100.

CONCLUSIONS

This paper presents for the first time the results of a study of heat transfer during boiling in thin horizontal layers of dielectric liquid HFE-7100 on a microstructured capillary-porous stainless steel coating. Comparison of the values of the temperature pressure and the heat transfer coefficient on capillary-porous coatings and a smooth surface shows that in HFE-7100 layers with height below 6 mm, the heat transfer regime changes from pool boiling to boiling in thin layers of liquid. It was found that the temperature difference achieved in a liquid layer 6 mm high on a capillary-porous coating at the heat flux density $q \sim 100$ kW/m^2 was six times less than that on the smooth surface. Comparison of the obtained experimental data with the data of other researchers shows that the HTC and CHF values on the smooth surface made of stainless steel are lower than those on the smooth surface made of copper. The geometric parameters chosen in this work and the material of the capillary-porous coating made of stainless steel made it possible to obtain high values of the heat transfer coefficient during boiling of HFE-7100 ($\alpha \sim 33$ kW/(m^2·K)).

NOTATIONS

a—coefficient of thermal diffusivity of liquid, m^2/s;

A—amplitude, μm;

$b = 1 + 10\left(\dfrac{\rho_v}{\rho_l - \rho_v}\right)^{2/3}$—dimensionless complex;

c_p—specific heat capacity, J/(kg·K);

C_s—correction factor;

C_{sf}—constant;

d—diameter, m;

d_0—bubble separation diameter, m;
g—free fall acceleration, m^2/s;
h—liquid layer height, m;
h_{lg}—latent heat of vaporization, J/kg;
$K_t = \dfrac{(h_{lg}\rho_v)^2 l_\sigma}{c_p T_s \rho_l \sigma}$—Peclet criterion;
$l_\nu = \left(\dfrac{\nu^2}{g\,(1-\rho_v/\rho_l)}\right)^{1/3}$—viscosity-gravitational constant of liquid, m;
$l_\sigma = \sqrt{\dfrac{\sigma}{g\,(\rho_l-\rho_v)}}$—capillary constant, m;
M—molar mass, kg/mol;
$Nu = \dfrac{\alpha l_\sigma}{\lambda_l}$—Nusselt criterion;
P—pressure, Pa;
$\mathrm{Pr} = \dfrac{\nu_l}{a_l}$—Prandtl criterion;
q—heat flux density, W/m^2;
R—universal gas constant, J/(mol·K);
R_a—surface roughness, μm;
$\mathrm{Re}_* = \dfrac{q l_\sigma}{h_{lg}\rho_v\nu_l}$—Reynolds criterion;
$\overline{R_z} = \dfrac{R_z}{l_\nu}$—dimensionless roughness;
T—temperature, °C, K;
$\Delta T = T_w - T_s$—temperature difference, °C, K;
x—horizontal coordinate;
$X = \dfrac{\lambda_l c_{pl}\rho_l}{\lambda_w c_{pw}\rho_w}$—dimensionless complex;
z—vertical coordinate;
α—heat transfer coefficient, $W/(m^2\cdot K)$;
$\gamma = \sqrt{\dfrac{\lambda_w c_{pw}\rho_w}{\lambda_l c_{pl}\rho_l}}$—complex;
θ—contact angle of wetting, °;
θ_{pr}—instrumental uncertainty of temperature measurement with thermocouple, °C;
λ—thermal conductivity coefficient, W/(m·K);
λ_m—coating modulation wavelength, mm;
μ—dynamic viscosity of liquid, Pa·s;
ν—kinematic viscosity of liquid, m^2/s;
ρ—density, kg/m^3;
σ—surface tension, N/m;
σ_{T_W}—residual variance for determination of parameter T_w;

Subscripts and Superscripts

l—liquid;
s—parameter on saturation line;
v—vapor;
w—parameter relating to heating surface.

FUNDING

The study was supported by a grant from the Russian Science Foundation (project no. 23-19-00245).

CONFLICT OF INTEREST

The authors of this work declare that they have no conflicts of interest.

REFERENCES

1. Leong, K.C., Ho, J.Y., and Wong, K.K., A Critical Review of Pool and Flow Boiling Heat Transfer of Dielectric Fluids on Enhanced Surfaces, *Appl. Therm. Eng.*, 2017, vol. 112, pp. 999–1019; https://doi:10.1016/j.applthermaleng.2016.10.138
2. Liang, G. and Mudawar, I., Review of Pool Boiling Enhancement by Surface Modification, *Int. J. Heat Mass Transfer*, 2019, vol. 128, pp. 892–933; https://doi:10.1016/j.ijheatmasstransfer.2018.09.026
3. Sajjad, U., Sadeghianjahromi, A., Ali, H.M., and Wang, C.C., Enhanced Pool Boiling Of Dielectric and Highly Wetting Liquids—A Review on Surface Engineering, *Appl. Therm. Eng.*, 2021, vol. 195, p. 117074; https://doi.org/10.1016/j.applthermaleng.2021.117074
4. Zhang, C., Sun, X., Han, Z., Li, X., and Dong, J., Energy Saving Potential Analysis of Twophase Immersion Cooling System with Multi-Mode Condenser, *Appl. Therm. Eng.*, 2023, vol. 219, p. 119614; https://doi.org/10.1016/j.applthermaleng.2022.119614
5. Pavlenko, A.N., Zhukov, V.I., and Shvetsov, D.A., Crisis Phenomena and Heat-Transfer Enhancement during Boling and Evaporation in Horizontal Liquid Films (Review), *Thermal Engin.*, 2022, vol. 69, no. 11, pp. 886–901; https://doi.org/10.1134/S0040601522110076
6. Nishikawa, K., Kusuda, H., Yamasaki, K., and Tanaka, K., Nucleate Boiling at Low Liquid Levels, *Bull. JSME*, 1967, vol. 10, pp. 328–338; https://doi.org/10.1299/jsme1958.10.328
7. Kopchikov, I.A., Voronin, G.I., Kolach, T.A., Labuntsov, D.A., and Lebedev, P.D., Liquid Boiling in a Thin Film, *Int. J. Heat Mass Transfer*, 1969, vol. 12, no. 7, pp. 791–796; https://doi.org/10.1016/0017-9310(69)90182-3
8. Grigor'ev, V.A. and Dudkevich, A.S., Boiling of Cryogenic Liquids in a Thin Film, *Teploenergetika*, 1970, no. 12, pp. 54–57.
9. Grigor'ev, V. A., Dudkevich, A.S., and Pavlov, Yu.M., Boiling of Cryogenic Liquids in a Thin Film, *Vopr. Radioelektron., Ser.: Tepl. Rezhimy, Termostatirovanie Okhlazhd. Radioelektron. Appar.*, 1970, no. 1, pp. 83–90.
10. Grigor'ev, V.A., Pavlov, Yu.M., and Ametistov, E.V., *Kipenie kryogennykh zhidkostei* (Boiling of Cryogenic Liquids), Moscow: Energiya, 1977.
11. Marto, P.J., Mackenzie, D.K., and Rivers, A.D., Nucleate Boiling in Thin Liquid Films, *AIChE Symp. Ser.*, 1977, vol. 73, no. 164, pp. 228–235.
12. Tolubinskii, V.I., Antonenko, V.A., and Ostrovskii, Y.N., Effect of the Height of a Liquid Layer on Acting Nucleation Sites, *Inzh.-Fiz. Zh.*, 1977, vol. 32, no. 1, pp. 13–17.
13. Tolubinskii, V.I., *Teploobmen pri kipenii* (Heat Transfer during Boiling), Kiev: Naukova dumka, 1980.
14. Tolubinskii, V.I., Antonenko, V.A., Ostrovskii, I.N., and Shevchuk, E.N., Heat Flux Limit in Evaporation of Liquid in Capillary Wicks of Low-Temperature Heat Pipes, *High Temp.*, 1980, vol. 18, no. 2, pp. 367–373.
15. Pioro, I.L., Experimental Evaluation of Constants for the Rohsenow Pool Boiling Correlation, *Int. J. Heat Mass Transfer*, 1999. vol. 42, no. 11, pp. 2003–2013; https://doi.org/10.1016/S0017-9310(98)00294-4
16. Pioro, I.L., Rohsenow, W., and Doerffer, S.S., Nucleate Pool Boiling Heat Transfer. I: Review of Parametric Effects of Boiling Surface, *Int. J. Heat Mass Transfer*, 2004, vol. 47, no. 23, pp. 5033–5044; https://doi.org/10.1016/j.ijheatmasstransfer.2004.06.019
17. Shukla, M.Y. and Kandlikar, S.G., Influence of Liquid Height on Bubble Coalescence, Vapor Venting, Liquid Return, and Heat Transfer in Pool Boiling, *Int. J. Heat Mass Transfer*, 2021, vol. 173, p. 121261; https://doi.org/10.1016/j.ijheatmasstransfer.2021.121261
18. Dong, Y., Yu, Y., Ibrahim, A., Hu, X., and Hao, Y., Influence of Liquid Height on Pool Boiling Heat Transfer over Open Rectangular Microchannels, *Appl. Therm. Eng.*, 2023, vol. 228, p. 120453; https://doi.org/10.1016/j.applthermaleng.2023.120453
19. Gogonin, I.I., Dorokhov, A.R., and Zhukov, V.I., Study of Evaporation from a Thin Oil Layer under Vacuum Conditions, *Izv. Sib. Otd. Akad. Nauk SSSR, Ser.Tekh. Nauk*, 1989, no. 3, pp. 8–13.
20. Zhukov, V.I., Enhanced Heat Transfer under Conditions of Liquid Boiling in a Thin Layer at Reduced Pressure, *Theor. Found. Chem. Eng.*, 2011, vol. 45, no. 5, pp. 690–694.

21. Zhukov, V.I. and Pavlenko, A.N., Critical Phenomena at Evaporation in a Thin Liquid Layer at Reduced Pressures, *J. Eng. Therm.*, 2013, vol. 22, no. 4, pp. 257–287; https://doi.org/10.1134/S1810232813040012
22. Zhukov, V.I., Pavlenko, A.N., Nagaitseva, Y.V., and Weiss, D., Effect of the Layer Height on Heat Transfer and the Critical Heat Flux in Evaporation of a Fluid under Low Pressures, *High Temp.*, 2015, vol. 53, pp. 690–696; https://doi.org/10.1134/S0018151X15050284
23. Zhukov, V.I. and Pavlenko, A.N., Effect of the Height of the Horizontal Layer of Liquid on the Development of Critical Phenomena in Evaporation at Reduced Pressures, *Heat Transfer Res.*, 2018, vol. 49, no. 11, pp. 979–990; https://doi.org/10.1615/HeatTransRes.2017016778
24. Zhukov, V.I. and Pavlenko, A.N., Heat Transfer and Critical Phenomena During Evaporation and Boiling in a Thin Horizontal Liquid Layer at Low Pressures, *Int. J. Heat Mass Transfer*, 2018, vol. 117, pp. 978–990; https://doi.org/10.1016/j.ijheatmasstransfer.2017.10.060
25. Zhukov, V.I. and Pavlenko, A.N., The Mechanism of Surface Cooling by a Horizontal Layer of Liquid Evaporating at Low Reduced Pressures, *AIP Adv.*, 2021, vol. 11, no. 1, pp. 015341; https://doi.org/10.1063/5.0023668
26. Brester, A.E., Shvetsov, D.A., Zhukov, V.I., and Pavlenko, A.N., Heat Transfer during Evaporation/Boiling of Horizontal Layers of Liquid at Low Pressure, *J. Eng. Therm.*, 2023, vol. 32, no. 3, pp. 415–445; https://doi.org/10.1134/S1810232823030025
27. Aleshin, A.A., Kuzma-Kichta, Yu.A., Moskvin, V.N., and Sorokin, D.N., Study of Heat Transfer in Vapor Generation on the Surface with a Porous Coating, *High Temp.*, 1980, vol. 18, no. 5, pp. 1098–1101.
28. Kuzma-Kichta, Y.A., Moskvin, V.N., and Sorokin, D.N. Study on Heat Transfer in Water Boiling on a Surface with Porous Coating at a Wide Pressure Range, *Teploenergetika*, 1982, no. 3, pp. 52–53.
29. Roizen, L.I., Rachitskii, D.G., Rubin, I.R., Vertogradskaya, L.M., Yudina, L.A., and Pypkina, M.B., Heat-Transfer with Boiling of Nitrogen and Freon-113 on Porous Metallic Coatings, *High Temp.*, 1982, vol. 20, no. 2, pp. 304–310.
30. Borsenko, V.I. and Malyshenko, S.P., Mechanisms of Phase Exchange under Conditions of Boiling on Surfaces with Porous Coatings, *High Temp.*, 2001, vol. 39, no. 5, pp. 769–776.
31. Liter, S.G. and Kaviany, M., Pool-Boiling CHF Enhancement by Modulated Porous-Layer Coating: Theory and Experiment, *Int. J. Heat Mass Transfer*, 2001, vol. 44, no. 22, pp. 4287–4311; https://doi.org/10.1016/S0017-9310(01)00084-9
32. Min, D.H., Hwang, G.S., Usta, Y., Cora, O.N., Koc, M., and Kaviany, M., 2-D and 3-D Modulated Porous Coatings for Enhanced Pool Boiling, *Int. J. Heat Mass Transfer*, 2009, vol. 52, pp. 2607–2613; https://doi.org/10.1016/j.ijheatmasstransfer.2008.12.018
33. Ji, X., Xu, J., Zhao, Z., and Yang, W., Pool Boiling Heat Transfer on Uniform and Non-Uniform Porous Coating Surfaces, *Exp. Thermal Fluid Sci.*, 2013, vol. 48, pp. 198–212; https://doi.org/10.1016/j.expthermflusci.2013.03.002
34. Zhang, C., Zhang, L., Xu, H., Li, P., and Qian, B., Performance of Pool Boiling with 3D Grid Structure Manufactured by Selective Laser Melting Technique, *Int. J. Heat Mass Transfer*, 2019, vol. 128, pp. 570–580; https://doi.org/10.1016/j.ijheatmasstransfer.2018.09.021
35. Elkholy, A. and Kempers, R., Enhancement of Pool Boiling Heat Transfer Using 3D-Printed Polymer Fixtures, *Exp. Thermal Fluid Sci.*, 2020, vol. 114, p. 110056; https://doi.org/10.1016/j.expthermflusci.2020.110056
36. Zhukov, V.I., Pavlenko, A.N., and Shvetsov, D.A., The Effect of Pressure on Heat Transfer at Evaporation/Boiling in Horizontal Liquid Layers of Various Heights on a Microstructured Surface Produced by 3D Laser Printing, *Int. J. Heat Mass Transfer*, 2020, vol. 163, p. 120488; https://doi.org/10.1016/j.ijheatmasstransfer.2020.120488
37. Shvetsov, D.A., Pavlenko, A.N., Brester, A.E, and Zhukov, V.I., Inversion of the Boiling Curve on Microstructured Porous Coatings, *High Temp.*, 2023, vol. 61, no. 3, pp. 405–409; https://doi.org/10.31857/S0040364423020163
38. Wallington, T.J., Schneider, W.F., Sehested, J., Bilde, M., Platz, J., Nielsen, O.J., Christensen, L.K., Molina, M.J., Molina, L.T., and Wooldridge, P.W., Atmospheric Chemistry of HFE-7100 ($C_4F_9OCH_3$): Reaction with OH Radicals, UV Spectra and Kinetic Data for $C_4F_9OCH_2$ and $C_4F_9OCH_2O_2$ Radicals, and the Atmospheric Fate of C_4F9OCH_2O Radicals, *J. Phys. Chem. A*, 1997, vol. 101, pp. 8264–8274; https://doi.org/10.1021/jp971353w
39. El-Genk, M.S. and Bostanci, H., Saturation Boiling of HFE-7100 from a Copper Surface, Simulating a Microelectronic Chip, *Int. J. Heat Mass Transfer*, 2003, vol. 46, no. 10, pp. 1841–1854; https://doi.org/10.1016/S0017-9310(02)00489-1
40. Liu, J.W., Lee, D.J., and Su, A., Boiling of Methanol and HFE-7100 on Heated Surface Covered with a Layer of Mesh, *Int. J. Heat Mass Transfer*, 2001, vol. 44, no. 1, pp. 241–246; https://doi.org/10.1016/S0017-9310(00)00078-8

41. El-Genk, M.S. and Parker, J.L., Enhanced Boiling of HFE-7100 Dielectric Liquid on Porous Graphite, *Energy Convers. Manag.*, 2005, vol. 46, no. 15–16, pp. 2455–2481; https://doi.org/10.1016/j.enconman.2004.11.012
42. Thiagarajan, S.J., Yang, R., King, C., and Narumanchi, S., Bubble Dynamics and Nucleate Pool Boiling Heat Transfer on Microporous Copper Surfaces, *Int. J. Heat Mass Transfer*, 2015, vol. 89, pp. 1297–1315; https://doi.org/10.1016/j.ijheatmasstransfer.2015.06.013
43. Hsu, Y., On the Size Range of Active Nucleation Cavities on a Heating Surface, *ASME J. Heat Mass Transfer*, 1962, vol. 84, no. 3, pp. 207–213; https://doi.org/10.1115/1.3684339
44. Manetti, L.L., Moita, A.S.O.H., de Souza, R.R., and Cardoso, E.M., Effect of Copper Foam Thickness on Pool Boiling Heat Transfer of HFE-7100, *Int. J. Heat Mass Transfer*, 2020, vol. 152, p. 119547; https://doi.org/10.1016/j.ijheatmasstransfer.2020.119547
45. Kiyomura, I.S., Nunes, J.M., de Souza, R.R., Gajghate, S. S., Bhaumik, S., and Cardoso, E.M., Effect of Microfin Surfaces on Boiling Heat Transfer Using HFE-7100 as Working Fluid, *J. Brazilian Soc. Mech. Sci. Engin.*, 2020, vol. 42, pp. 1–13; https://doi.org/10.1007/s40430-020-02439-7
46. dos Santos Filho, E., Kiyomura, I.S., de Andrade, B.A., and Cardoso, E.M., Pool Boiling Performance of HFE-7100 on Hierarchically Structured Surfaces, *Case Stud. Thermal Engin.*, 2021, vol. 28, p. 101536; https://doi.org/10.1016/j.csite.2021.101536
47. Doran, B., Zhang, B., Walker, A., Pratik, K.C., Meng, W.J., and Moore, A.L., Experimental Determination of the Role of Increased Surface Area in Pool Boiling from Nanostructured Surfaces, *Exp. Thermal Fluid Sci.*, 2020, vol. 111, p. 109956; https://doi.org/10.1016/j.expthermflusci.2019.109956
48. Fan, S., Tong, W., and Duan, F., Nucleate Pool Boiling Heat Transfer Enhancement in Saturated Novec 7100 Using Titanium Dioxide Nanotube Arrays, *Int. Commun. Heat Mass Transfer*, 2021, vol. 122, p. 105166; https://doi.org/10.1016/j.icheatmasstransfer.2021.105166
49. Alvariño, P.F., Simón, M.L.S., dos Santos Guzella, M., Paz, J.M. A., Jabardo, J.M.S., and Gómez, L.C., Experimental Investigation of the CHF of HFE-7100 under Pool Boiling Conditions on Differently Roughened Surfaces, *Int. J. Heat Mass Transfer*, 2019, vol. 139, pp. 269–279; https://doi.org/10.1016/j.ijheatmasstransfer.2019.04.142
50. Fan, X., Gu, S., Lei, J., Luo, G., Meng, F., Wu, L., and Gu, S., Experimental and Analytical Study on the Influence of Saturation Pressure and Surface Roughness on Pool Boiling CHF of HFE-7100, *Int. J. Chem. Engin.*, 2022; https://doi.org/10.1155/2022/4875208
51. Mlakar, G., Huang, C.N., and Kharangate, C., Effects of Surface Modifications on Pool Boiling Heat Transfer with HFE-7100, *Int. J. Thermofluids*, 2023, vol. 17, p. 100286; https://doi.org/10.1016/j.ijft.2023.100286
52. Jiang, Y., Zhou, G., Zhou, J., Zhou, F., and Huai, X., Saturated Pool Boiling Heat Transfer of HFE-7100 on Sintered Copper Powder and Wire Mesh Microporous Surfaces: A Comparison Study, *Appl. Therm. Eng.*, 2022, vol. 216, p. 119067; https://doi.org/10.1016/j.applthermaleng.2022.119067
53. Wu, F., Hisano, T., Umehara, Y., Takata, Y., and Mori, S., Improvement in the Onset of The Nucleate Pool Boiling of HFE-7100 with the Use of a Honeycomb Porous Plate and Heated Fine Wire, *Int. J. Heat Mass Transfer*, 2023, vol. 217, p. 124738; https://doi.org/10.1016/j.ijheatmasstransfer.2023.124738
54. Lum, L.Y.X., Leong, K.C., and Ho, J.Y., Optimizing Additively Manufactured Macro-Fin Structure Designs for Enhanced Pool Boiling of Dielectric Fluids, *Int. J. Heat Mass Transfer*, 2024, vol. 219, p. 124883; https://doi.org/10.1016/j.ijheatmasstransfer.2023.124883
55. Gogonin, I.I., *Heat Transfer in Nucleate Boiling*, Cambridge Scholars Publ., 2023.
56. 3M^{TM}Novec^{TM}Engineered Fluid HFE-7100 Physical Properties, 2002.
57. Rausch, M.H., Kretschmer, L., Will, S., Leipertz, A., and Fröba, A.P., Density, Surface Tension, and Kinematic Viscosity of Hydrofluoroethers HFE-7000, HFE-7100, HFE-7200, HFE-7300, and HFE-7500, *J. Chem. Engin. Data*, 2015, vol. 60, no. 12, pp. 3759–3765; https://doi.org/10.1021/acs.jced.5b00691
58. Lee, J. and Mudawar, I., Fluid Flow and Heat Transfer Characteristics of Low Temperature Two-Phase Micro-Channel Heat Sinks—Part 1: Experimental Methods and Flow Visualization Results, *Int. J. Heat Mass Transfer*, 2008, vol. 51, nos. 17/18, pp. 4315–4326; https://doi.org/10.1016/j.ijheatmasstransfer.2008.02.012
59. Bessmeltsev, V.P., Pavlenko, A.N., and Zhukov, V.I., Development of a Technology for Creating Structured Capillary-Porous Coatings by Means of 3D Printing for Intensification of Heat Transfer during Boiling, *Optoelectron, Instrum. Data Process*, 2019, vol. 55, no. 6, pp. 554–563.
60. Zubchenko, A.S., Koloskov, M.M., Kashirskii, Yu.V., et al., *Marochnik stalei i splavov* (Guide for Steels and Alloys), Moscow: Mashinostroenie, 2003.
61. Oleinik, B.P., Surin, V.G., and Petrova, O.K., Research of Heat Conductivity of Stainless and Low-Carbon Steels, *High Temp.*, 1985, vol. 23, no. 3, pp. 500–505.
62. Gogonin, I.I., The Dependence of Boiling Heat Transfer on the Properties and Geometric Parameters of Heat-Transfer Wall, *High Temp.*, 2006, vol. 44, no. 6, pp. 913–921; https://doi.org/10.1007/s10740-006-0110-3

63. Li, Y.Y., Chen, Y.J., and Liu, Z.H., A Uniform Correlation for Predicting Pool Boiling Heat Transfer on Plane Surface with Surface Characteristics Effect, *Int. J. Heat Mass Transfer*, 2014, vol. 77, pp. 809–817; https://doi.org/10.1016/j.ijheatmasstransfer.2014.05.060
64. Rohsenow, W.M., A Method of Correlating Heat-Transfer Data for Surface Boiling of Liquids, *Trans. Am. Soc. Mechan. Engin.*, 1952, vol. 74, no. 6, pp. 969–975; https://doi.org/10.1115/1.4015984
65. Stephan, K. and Abdelsalam, M., Heat-Transfer Correlations for Natural Convection Boiling, *Int. J. Heat Mass*, 1980, vol. 23, no. 1, pp. 73–87; https://doi.org/10.1016/0017-9310(80)90140-4
66. Song, Y., Díaz-Marín, C.D., Zhang, L., Cha, H., Zhao, Y., and Wang, E.N., Three-Tier Hierarchical Structures for Extreme Pool Boiling Heat Transfer Performance, *Adv. Mater.*, 2022, vol. 34, no. 32, p. 2200899; https://doi.org/10.1002/adma.202200899
67. Zhukov, V.I. and Pavlenko, A.N., Symmetry of Structures under Two-Dimensional Instability in a Finite-Height Horizontal Layer of Boiling Liquid, *Symmetry*, 2023, vol. 15, no. 9, p. 1792; https://doi.org/10.3390/sym15091792